Flow Boiling in a Micro-Channel Coated With Carbon Nanotubes

Vikash Khanikar, Issam Mudawar, and Timothy S. Fisher

***Abstract*—This study examines the heat transfer enhancement attributes of carbon nanotubes (CNTs) applied to the bottom wall of a shallow rectangular micro-channel. Using deionized water as working fluid, experiments were performed with both a bare copper bottom wall and a CNT-coated copper wall. Boiling curves were generated for both walls, aided by high-speed video analysis of interfacial features. CNT arrays promoted earlier, abundant and intense bubble nucleation at low mass velocities, consistent with findings from previous pool boiling studies. However, high mass velocities compromised or eliminated altogether any enhancement in the nucleate boiling region. The enhancement achieved at low mass velocities appears to be the result of deep, near-zero-angle cavities formed by the mesh of CNT arrays. On the other hand, high mass velocities tend to fold the CNTs upon the wall, greatly reducing the depth of the CNT-mesh-induced cavities, and compromising the effectiveness of CNTs at capturing embryos and sustaining the bubble nucleation process. CHF enhancement was also achieved mostly at low mass velocities. It is postulated CNT arrays enhance CHF by increasing the heat transfer area as well as by serving as very high conductivity fins that penetrate into the cooler, bulk liquid flow and take advantage of the liquid subcooling away from the wall. While these mechanisms are prevalent at low velocities, they are both weakened, especially the fin effect, at high mass velocities because of the folding of CNT arrays upon the wall.**

NOMENCLATURE

A_{ch}	cross-sectional area of micro-channel;
A_t	bottom wall area of micro-channel (also top surface area of copper block);
CHF	critical heat flux;
D_h	hydraulic diameter;
G	mass velocity;
H_{ch}	height of micro-channel;
H_{th}	distance between thermocouple and bottom wall of micro-channel;
k_s	thermal conductivity of copper block;
L	length of micro-channel;
$\dot{m}$	mass flow rate of coolant;
P	pressure;
q''	heat flux from bottom wall of micro-channel (based on A_t);
q''_m	critical heat flux from bottom wall of micro-channel (based on A_t);
Re	Reynolds number;
T	temperature;
ΔT_{sub}	subcooling, $T_{sat} - T_f$;
T_{tci}	temperature measured by thermocouple tci $(i = 1 - 4)$;
$T_{w,tci}$	surface temperature at $z_{tci} (i = 1 - 4)$;
W_{ch}	width of micro-channel;
z	stream-wise location.

SUBSCRIPTS

ch	micro-channel;
f	liquid;
in	inlet;
out	outlet;
s	solid;
sat	saturation;
tci	thermocouple i $(i = 1 - 4)$;
w	bottom wall of micro-channel.

Manuscript received April 04, 2008; revised July 16, 2008. Current version published August 26, 2009. This work was recommended by Associate Editor Mehmet Arik upon evaluation of the reviewers comments.

The authors are with the Boiling and Two-Phase Flow Laboratory (BTPFL) and Birck Nanotechnology Center, West Lafayette, IN 47907-2088 USA (e-mail: mudawar@ecn.purdue.edu).

Digital Object Identifier 10.1109/TCAPT.2009.2015232

I. INTRODUCTION

FOR a half-century, the quest for superior electronic device performance has been met by the continued successes on two fronts: microminiaturization and integration of an increasing number of components in a single device. Accompanying these successes, however, has been a compounding problem of increased heat dissipation per unit device surface area. While device manufacturers have made many strides to reduce the heat dissipation, efforts have often been short-lived.

To combat the heat dissipation problem, various air-cooling technologies were initially developed, whose performance was gradually enhanced by using more powerful fans and complex fin structures. Once these technologies began to fall short of the required heat dissipation for high-end devices, interest shifted to liquid cooling technologies to capitalize upon the superior thermophysical properties of liquids compared to air. Yet even these liquid-cooling technologies are incapable of meeting the

heat dissipation requirements of today's high-performance devices. Researchers are presently placing emphasis on the implementation of phase-change cooling schemes, especially those involving high coolant velocities, such as micro-channel, jet and spray [1].

Flow boiling in a rectangular channel is a simple, yet effective means for cooling multi-device circuit boards, especially those that are parallel-mounted in an electronic enclosure. Mudawar and Maddox [2] investigated subcooled flow boiling on a simulated electronic chip inside a vertical rectangular channel. Increasing inlet liquid velocity enhanced the single-phase heat transfer coefficient, delayed the onset of boiling, and increased the critical heat flux (CHF). Near CHF, bubbles coalesced into fairly continuous vapor blankets that inhibited liquid access to the heated wall, but the shape and size of the vapor blankets was highly velocity-dependent. Low flow velocities tolerated appreciable vapor growth, causing a single continuous vapor blanket to form and hover over the entire heated wall. At high velocities, interfacial instabilities fragmented the vapor blanket, resulting a series of shorter, discrete blankets that covered the wall as CHF ensued. Mudawar and Maddox also showed CHF can be greatly enhanced by increasing the subcooling of the incoming liquid. Cooler liquid can absorb a significant amount of sensible heat before undergoing evaporation. Furthermore, higher subcooling decreases vapor bubble size by condensation, bringing the bulk liquid closer to the heated wall. Willingham and Mudawar [3] performed similar flow boiling experiments in rectangular channels with different heights. Decreasing the channel height increased the vapor void fraction as well as caused bubbles to flatten and spread laterally.

Two-phase micro-channel flow is an extreme form of channel flow boiling, where hydraulic diameter is reduced to the range of 100 to 1000 μm [1]. The advantages of micro-channel flow are quite obvious for laminar single-phase flow, where the heat transfer coefficient is inversely proportional to hydraulic diameter. For two-phase flow, the merits of micro-channel flow are closely associated with fast fluid acceleration along the micro-channel and close proximity of the bulk liquid to the heated wall. As explained by Qu and Mudawar [4]–[6], two-phase micro-channel flow greatly enhances the convective heat transfer coefficient and the uniformity of both the coolant and wall temperatures, as well as requires a smaller coolant flow rate to dissipate a given amount of heat compared to single-phase micro-channel flow. However, these advantages are sometimes realized at the expense of increased pressure drop. Steinke and Kandlikar [7] also investigated flow boiling characteristics of water in micro-channels. They observed similar flow characteristics such as flow reversal at high heat fluxes and dry-out in the micro-channel before attaining CHF. Wang *et al.* [8] also reported similar observations in their experimental study of stable and unstable flow boiling in parallel micro-channels and a single micro-channel. They categorized three different boiling modes depending on the heat-to-mass velocity ratio: stable flow boiling regime with no periodic oscillation, and unstable flow boiling regimes with short period and long-period oscillation. The present study explores the concept of further enhancing two-phase micro-channel cooling performance by the use of carbon nanotubes (CNTs).

A. Heat Transfer Enhancement With Carbon Nanotubes

CNTs have received considerable attention amongst researchers worldwide because of their unique electrical, thermal and mechanical properties. CNTs are extremely thin tubes of graphitic carbon with outer diameters ranging from 1 to 100 nm and lengths from 1 to 50 μm. CNTs exist in either single-walled (SWNT) or multi-walled (MWNT) forms. SWNTs are made from a single graphene sheet, made up of hexagonally arranged groups of carbon atoms, whereas MWNTs are made from multiple graphene sheets. Kim *et al.* [9] showed that MWNTs possess thermal conductivities in excess of 3000 W/m.K, which renders MWNTs very attractive for heat transfer applications.

Recently, Ujereh *et al.* [10] explored the enhancement benefits of CNTs to pool boiling. CNT arrays proved effective in reducing the incipient boiling superheat and enhancing the nucleate boiling heat transfer coefficient for both silicon and copper walls in FC-72. These advantages were attributed to the effectiveness of CNTs at both initiating and sustaining the nucleation process; better nucleate boiling heat transfer was also believed to result from increased surface area. CNT-coated walls were found to provide an abundance of bubble nucleation sites by modifying the process of vapor embryo entrapment, especially for dielectric coolants. These coolants possess unusually small contact angles, which, for non-coated walls, allow liquid to easily penetrate and flood wall cavities, inhibiting the formation of the large-sized vapor embryos necessary to both initiating and sustaining the nucleation process. The CNT coating, the parallel vertical CNTs as well as the mesh of CNTs create deep, near-zero-angle cavities that are ideal for embryo formation, especially for the low contact angle coolants. Ujereh *et al.* also demonstrated significant CHF enhancement with CNTs for both silicon and copper walls because of the aforementioned increase in surface area. Launay *et al.* [11] showed that CNTs are effective in enhancing pool boiling heat transfer of PF-5060 when compared to a smooth silicon wall only at very low superheats, and their performance is highly degraded near CHF. They suggested that the enhancement benefits of CNTs could be compromised by the contact resistance between the CNTs and the wall. Differences in nucleate boiling performance between the studies of Ujereh *et al.* and Launay *et al.* can be attributed to differences in the CNT growth process and anchoring to the surface; both have a strong bearing on the contact resistance. Dujardin *et al.* [12] showed that fluids such as water and most low surface tension fluids can effectively wet and penetrate CNTs, which provides an ideal environment for increased bubble nucleation sites.

As discussed earlier, many innovative concepts have been developed and tested that rely on a copper micro-channel heat sink to aid heat removal form an electronic device. The work presented in this paper is the first effort focusing on a particular surface enhancement technique that investigates how single-phase and two-phase heat sink performance maybe enhanced by coating the bottom wall of a single micro-channel with CNTs. The present study aims to explore the heat transfer benefits of CNTs to flow boiling of water in a micro-channel. Instead of using a heat sink containing a large number of parallel micro-channels, this study utilizes a single, wide rectangular micro-

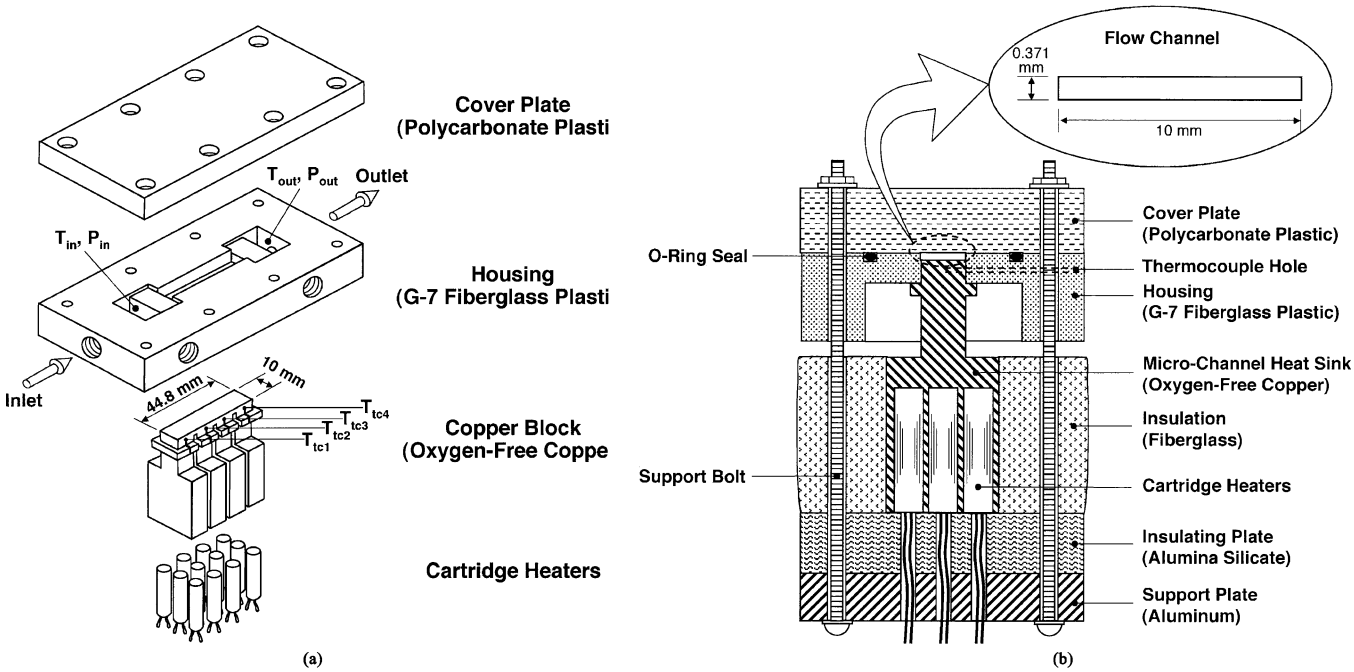

Fig. 1. (a) Main parts and (b) sectional assembly view of test module.

channel whose bottom copper heated wall is coated with CNTs. This geometry provides convenient optical access to the boiling surface as well as helps isolate the enhancement effects of CNTs from those of the copper sidewalls (fins) in a conventional multi-channel heat sink. Boiling curves are generated for both a bare copper wall and a CNT-coated wall to assess the influence of CNTs on the onset of boiling, the nucleate boiling heat transfer coefficient, and CHF.

II. Experimental Methods

A. Test Module

Fig. 1(a) illustrates the construction of the test module, which consists of an oxygen-free copper block, a G-7 fiberglass plastic housing, a polyethermide thermoplastic (GE Ultem 1000) cover plate, and twelve cartridge heaters. The top 44.8×10 mm^2 surface of the copper block constitutes the heated bottom wall for the micro-channel. The cartridge heaters are inserted into bores in the underside of the copper block to provide heat to the heated wall. Three deep, narrow slots are cut from the underside through most of the copper block to ensure a 1-D conduction heat path to the channel's bottom wall. This uniformity was validated by a numerical model of the entire copper block. The central portion of the G-7 housing is machined out to accommodate the top portion of the copper block. The housing contains both an upstream plenum and a downstream plenum to ensure uniform flow distribution. Each plenum has both a deep cavity and a shallow cavity. A small protruding platform around the periphery of the copper block ensures that the heated wall is flush with the base of the shallow cavity in each plenum. The cartridge heaters are inserted into the underside of the copper block and held in place with the aid of a ceramic support plate. A thick G-10 fiberglass plastic plate is used to thermally insulate the underside of the test module.

TABLE I
Key Dimensions of Micro-Channel and Copper Block

W_{ch} [mm]	H_{ch} [mm]	L [mm]	H_{th} [mm]
10	0.371	44.8	1.24

A cross-sectional view of the assembled test module is shown in Fig. 1(b). The flow channel is 10-mm wide and 0.371-mm high. The size of the flow channel is selected to facilitate comparing the present data with those of the micro-channel test module used in a previous study by Qu and Mudawar [4]. Their module featured twenty-one 0.215-mm wide by 0.821-mm deep micro-channels, and had the same base heated area's length and width, 44.8 mm and 10 mm, respectively, as the present test module. With a height of 0.371 mm, the present flow channel has the same total flow area as Qu and Mudawar's micro-channel module, which provided equal values of mass velocity for the same to total mass flow rate.

As shown in Fig. 1(a), four type-K thermocouples are inserted in the copper block 1.13 mm below the heated wall to measure stream-wise wall temperature variations along the flow direction. These thermocouples are designated as *tc1* to *tc4* starting with the one closest to the micro-channel's inlet. The cartridge heaters are powered by a 0–110 VAC variac and their total heat dissipation measured by a wattmeter. The deep cavity in each plenum is instrumented with an absolute pressure transducer and a type-K thermocouple. Table I summarizes the key dimensions of the micro-channel and the copper block.

B. Flow Loop

Fig. 2 shows a schematic of the flow loop that is designed to deliver deionized water to the test module at the desired flow rate, pressure and temperature. The water is pumped from a

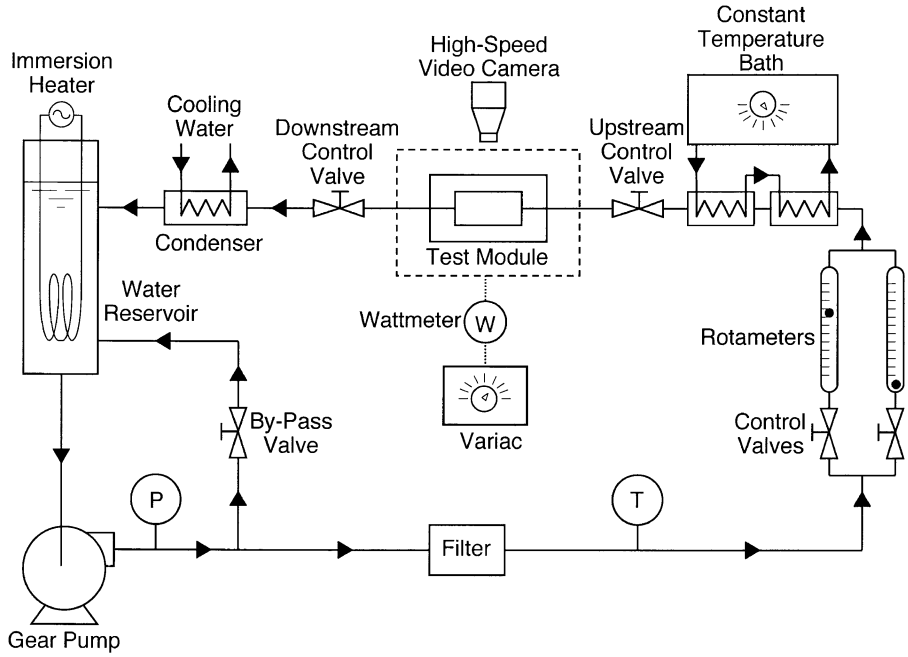

Fig. 2. Schematic of two-phase flow loop.

TABLE II
OPERATING CONDITIONS FOR PRESENT STUDY

Coolant	T_{in} [°C]	G [kg/m^2.s]	Re	P_{out} [bar]
Deionized Water	30	86, 228, 368	76 - 327	1.13
	60	86, 228, 368	131 - 562	1.13

reservoir through a filter, one of two rotameters, and two plate heat exchangers before entering the test module. Secondary water from a constant-temperature bath is circulated though the plate heat exchangers to help control the temperature of the deionized water at the inlet to the test module. Control valves situated both upstream and downstream of the test module are used to set the desired module outlet pressure as well as prevent any flow or pressure fluctuations in the module.

C. Experimental Procedure

Each test is characterized by a module inlet temperature, $T_{\rm in}$, module outlet pressure, $P_{\rm out}$, and mass velocity, G; the latter is the ratio of mass flow rate, $\dot{m}$, to the micro-channel's flow area of $A_{ch} = 10.0 \times 0.371$ mm^2. The tests were performed with a constant outlet pressure of $P_{\rm out} = 1.13$ bar, two inlet temperatures of $T_{\rm in} = 30^\circ$ and 60°C, (corresponding to inlet subcooling levels of $\Delta T_{\rm sub,in} = 71.0$–$73.6^\circ$ and 43.0–43.7°C, respectively; variations in subcooling are due to different module inlet pressures), and mass velocities in the range of $G =$ 86-368 kg/m^2.s. These are similar to the operating conditions of the previous study by Qu and Mudawar [4]. Table II summarizes the operating conditions of the present study. Heat flux, q'', from the heated wall is defined as the measured electrical power input to the cartridge heaters divided by the heated wall area of $A_t = 44.8 \times 10.0$ mm^2.

The deionized water was deaerated prior to each series of tests conducted the same day. The water was brought to a vigorous boil inside the reservoir for about two hours to purge any dissolved gases to the ambient, while the water was circulated through the loop. Subsequently, the flow loop's components were adjusted to achieve the desired operating conditions. Electrical power was then supplied to the test module's cartridge heaters in small increments. This required readjusting various loop controls to preserve the test's operating conditions. The power was increased again only after these conditions were ascertained and the copper block temperatures reached steady state. Before the new power increment, the electrical power input, the inlet and outlet pressures, $P_{\rm in}$ and $P_{\rm out}$, the inlet and outlet temperatures, $T_{\rm in}$ and $T_{\rm out}$, and the copper block temperatures, T_{tc1} to T_{tc4}, were all recorded using an HP data acquisition system interfaced to a PC. The test was terminated by turning off the electrical power input once a rapid unsteady temperature rise was detected in the copper block, signaling the commencement of CHF.

D. Measurement Uncertainty

Numerical simulation was used to ascertain the percentage of the electrical power input to the test module that was lost to the ambient rather than transferred to the liquid from the heated wall. A numerical 3D model of the test module was constructed in which electrical power input was simulated as a uniform heat flux along the walls of the cartridge heater bores. Because the two-phase heat transfer coefficient cannot be directly measured, numerical iteration was required. An initial value of the heat transfer coefficient was determined by equating the rate of heat transferred to the liquid to the electrical power input (*i.e.*, by assuming zero heat loss), and using the measured mean surface

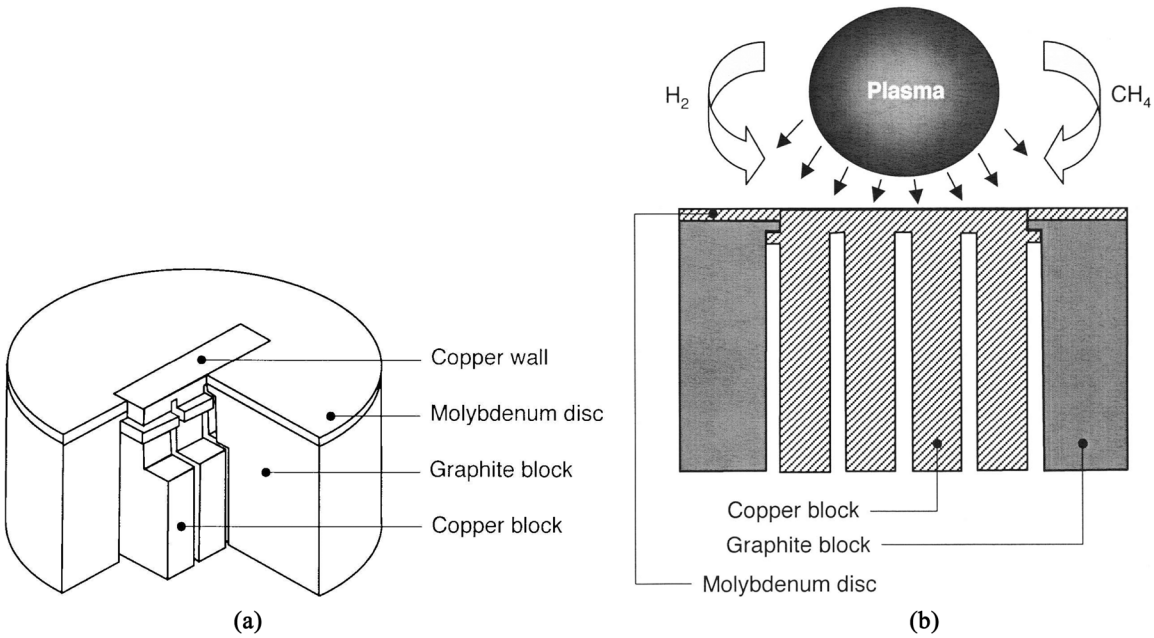

Fig. 3. (a) Schematic of graphite fixture. (b) Experimental setup for CNT growth in MPCVD reactor.

and mean fluid temperatures. This value was then adjusted numerically until the predicted mean temperature at the thermocouple plane matched the measured mean temperature. From the numerical results, maximum heat loss was estimated at 6 to 10% of the electrical power input for single-phase and two-phase conditions, respectively. Therefore, all heat flux data presented in this study are set equal to the total electrical power input divided by the area of the heated wall.

Additional measurements uncertainties are attributed to the instrumentation used in the study. The wattmeter used to measure the electrical power input has an accuracy of 0.5%. The uncertainties in the pressure and temperature measurements are estimated at 3.5% and $\pm 0.3^{\circ}$C respectively, and the rotameters 4%.

Two different surfaces were tested. The first is a bare copper wall that was vapor blasted to provide an abundance of surface cavities as large as 3 μm. The second is an identical copper surface that was coated with CNTs as described in Section III-E.

E. Carbon Nanotube Surface Preparation

CNT growth was achieved with the aid of a tri-layer metal catalyst [13] in combination with H_2 and CH_4 as feed gases reacted with the catalyst in a microwave plasma chemical vapor deposition chamber (MPCVD). Different metal catalysts have been used in the past for carbon nanotube growth. In this study, a tri-layer metal catalyst consisting of titanium, aluminum and iron provided good growth on the copper wall. The titanium under-layer provided surface bonding sites for CNTs that were well anchored to the copper surface. The anchoring of CNTs to the surface is crucial for two reasons. First, good anchoring greatly reduces thermal contact resistance between the CNTs and the surface, leading to minimal resistance to heat transfer [14]. Second, well-anchored CNTs possess greater resistance to detachment by shear forces exerted by the fluid flow.

The first step of the CNT growth involved cleaning the top wall of the test module's copper block in water and methanol. The copper wall was then placed in a three-target Varian electron-beam metal evaporation chamber. In the chamber, a 30-nm titanium layer was deposited first, followed sequentially by 15 nm of aluminum and 9 nm of iron. The purpose of the aluminum layer is to promote the segregation of annealed iron nanoparticles [15].

A SEKI AX5200S MPCVD reactor [16] was used for CNT growth. Because of the large size of the copper block, a graphite fixture was fabricated to shield the uncoated surfaces of the copper block from the microwave plasma, and also to prevent plasma concentration along the sharp metal edges. Shown in Fig. 3(a), the graphite fixture was machined from a solid cylinder that was hollowed to the outer dimensions of the copper block. All edges of the graphite fixture were carefully chamfered to prevent adverse plasma concentration. The copper wall penetrated a rectangular hole of the same size (44.8×10.0 mm^2) in the top surface of the graphite fixture. To concentrate the plasma directly above the test surface, a 3.175-mm thick chamfered molybdenum puck, also having a 44.8×10.0 mm^2 central rectangular hole, was placed atop the graphite fixture to produce a surface that was flush with the copper wall. The assembly, with the tri-layer metal catalyst deposited on the copper wall, was then placed on top of a graphite susceptor in the chamber. Fig. 3(b) shows a schematic of the experimental setup for CNT growth in the MPCVD reactor. The plasma was powered by a 1.5 kW (2.45 GHz) ASTex AX2100 microwave generator. Inductive substrate heating was supplied by a 3.5 kW radio-frequency coil and power supply beneath the susceptor.

The synthesis protocol used for CNT growth involved annealing, hydrogen plasma ignition, and introduction of a carbon-containing gas species. Before supplying the feed gases (H_2 and CH_4), the test surface was annealed in N_2 at 50 sccm for ten minutes using the induction heater. The N_2 feed was stopped

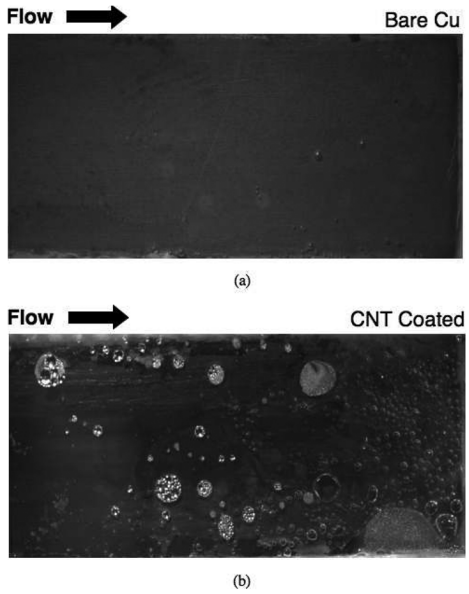

Fig. 4. Onset of boiling in downstream region of micro-channel at $G = 124$ kg/m^2.s and $T_{\rm in} = 30^\circ$C for (a) bare wall at $q'' = 24$ W/cm^2 and (b) CNT-coated wall at $q'' = 20.5$ W/cm^2.

when the temperature of the test surface was approximately 700°C as measured by a dual-wavelength Williamson pyrometer. Immediately thereafter, the chamber was evacuated, and then the H_2 was introduced at 50 sccm until the chamber pressure reached 10 torr. At this point, the plasma was ignited at 300 W, and then the CH_4 introduced at 10 sccm. With the plasma above the copper wall, the pyrometer indicated a temperature of approximately 800°C. The CNT synthesis process was terminated after ten minutes to achieve sufficient array height, and the reactor was evacuated. The sample was allowed to cool to room temperature before being removed from the chamber. The resulting CNT coating consists of MWCNTs with a diameter of about 60 nm.

III. Flow Visualization Results

High-speed video imaging was used to capture two-phase flow behavior in the micro-channel. A transparent cover plate for the test module provided optical access in a direction normal to the flow. At the heart of the video system is a Photron FASTCAM-Ultima APX \FM camera that was fitted with an array of high magnification lenses. Video sequences were captured for both the bare and CNT-coated walls for two mass velocities ($G = 124$ and 368 kg/m^2.s) at $T_{\rm in} = 30^\circ$ and 60°C.

A. Onset of Nucleate Boiling

Fig. 4 compares the onset of boiling on the bare and CNT-coated walls for $G = 124$ kg/m^2.s and $T_{\rm in} = 30^\circ$C. These and other photos discussed later must be referenced relative to the 10.00 mm width of the heated surface. For both walls, nucleation commenced in the downstream region of the micro-channel in the form of bubbles that nucleated mostly towards the sidewalls. However, boiling commenced on the CNT-coated wall at a lower heat flux and with much greater abundance and intensity.

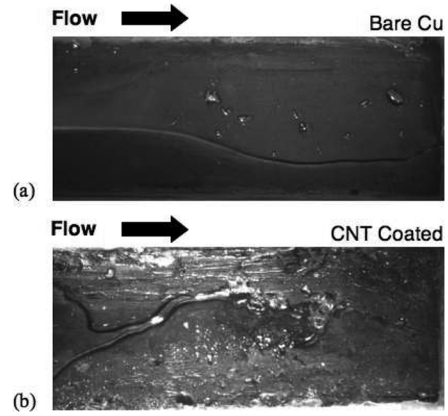

Fig. 5. Flow boiling pattern in downstream region of micro-channel at $G = 124$ kg/m^2.s and $T_{\rm in} = 60^\circ$C for (a) bare wall at $q'' = 19.6$ W/cm^2 and (b) CNT-coated wall at $q'' = 20.5$ W/cm^2.

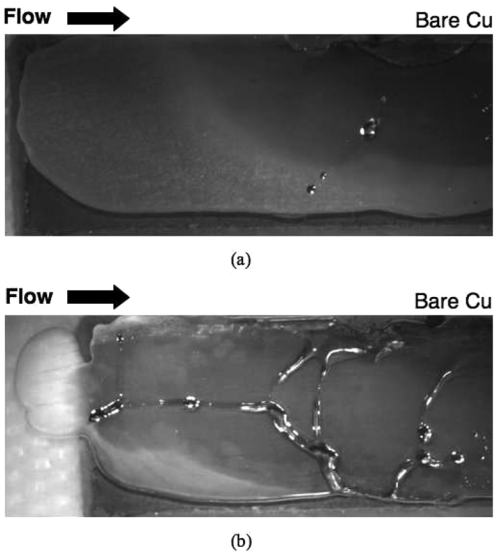

Fig. 6. Vapor back flow in upstream region of micro-channel for bare wall at $G = 368$ kg/m^2.s for (a) $T_{in} = 30^\circ$C and $q'' = 50.9$ W/cm^2 (close to CHF), and (b) $T_{in} = 60^\circ$C and $q'' = 53.1$ W/cm^2 (CHF).

B. Two-Phase Flow Pattern Development

At $G = 124$ kg/m^2.s, two-phase flow patterns and the transitions between patterns associated with increasing heat flux were very different for the bare wall and the CNT-coated wall. For the bare wall, there was a rapid transition from bubbly flow to slug flow followed by annular flow, eventually reaching dryout at CHF. Because of the large channel width, different flow patterns occurred side-by-side at the same axial location. Fig. 5(a) shows, for $G = 124$ kg/m^2.s and $T_{\rm in} = 60^\circ$C, a complex flow pattern in the downstream region of the micro-channel following a small increase in heat flux from the onset of boiling. A large slug-flow bubble is shown occupying a large portion of the cross-section with liquid flow prevailing over the remaining portion. Also visible are droplets that are entrained in the large bubble. For the CNT-coated wall, more intense nucleation upstream helped break the liquid flow following a small heat flux increment from the onset of boiling. Fig. 5(b) shows, for the downstream region of the CNT-coated wall, a single central

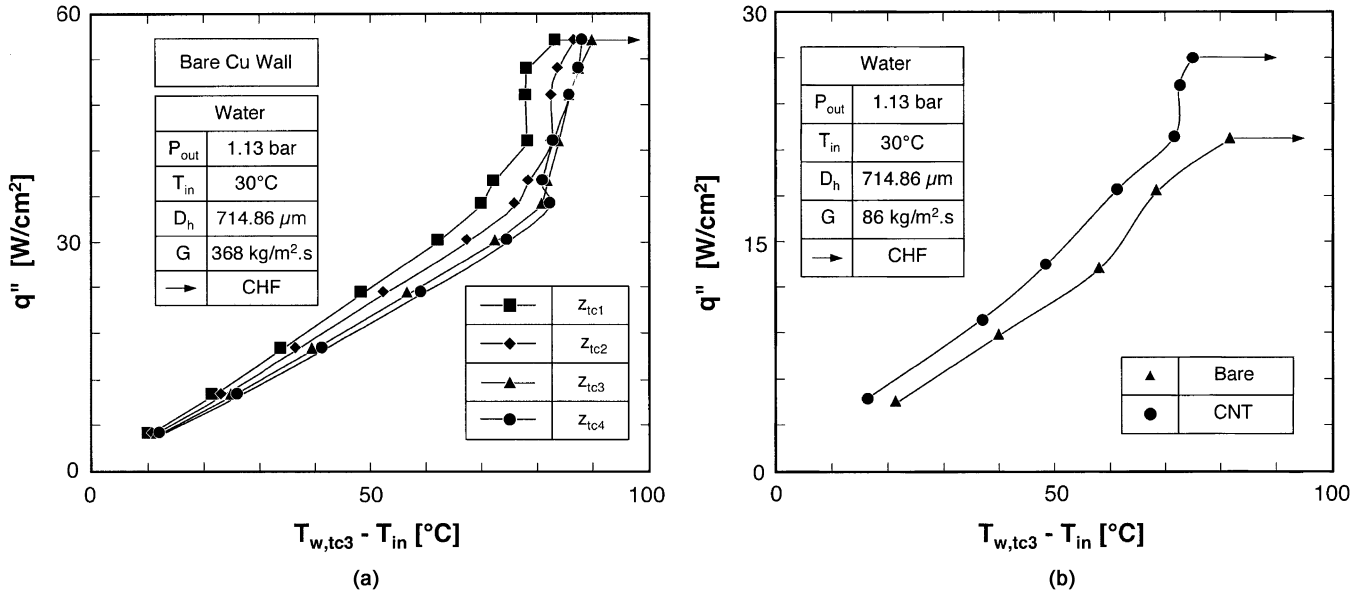

Fig. 7. Subcooled flow boiling curves measured at ztc1 to ztc4 for bare copper surface at $G = 368$ kg/m^2.s and $T_{in} = 30°$C.

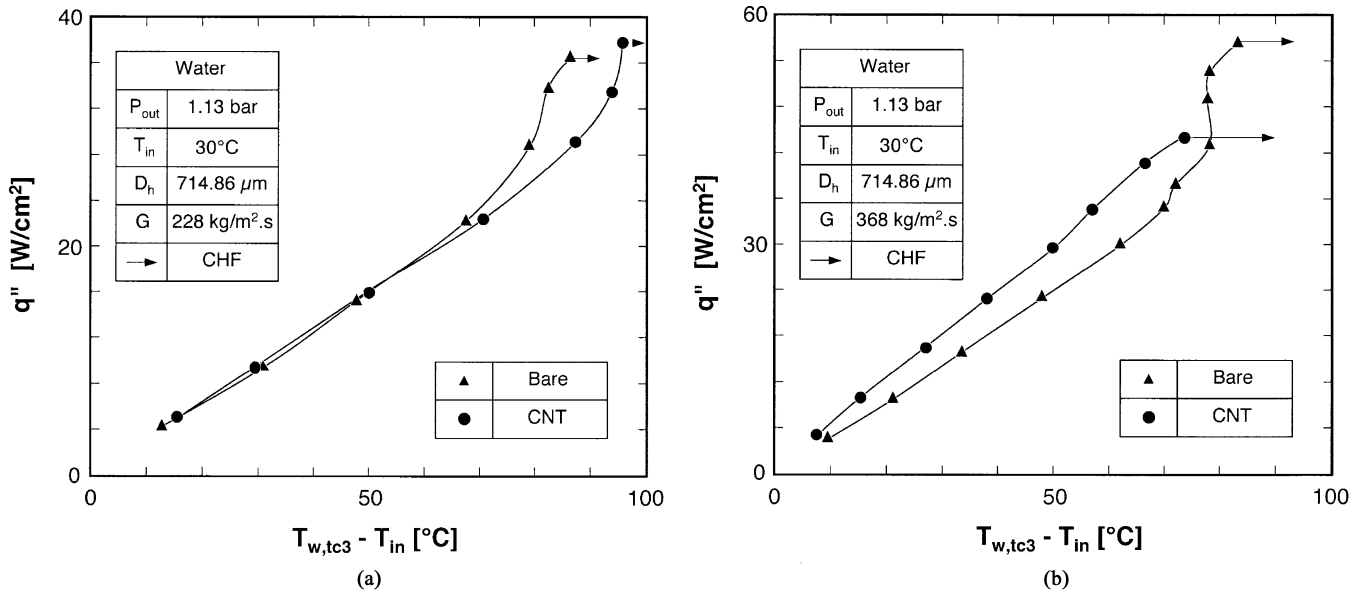

Fig. 8. Subcooled flow boiling curves measured at ztc3 for bare and CNT-coated walls at $T_{\rm in} = 30°$C for (a) $G = 86$ kg/m^2.s, (b) $G = 288$ kg/m^2.s, and (c) $G = 368$ kg/m^2.s.

liquid stream surrounded by predominantly annular flow containing entrained droplets.

C. Critical Heat Flux

For both the bare and CNT-coated walls, CHF was triggered by severe vapor backflow. Pressure measurements in both the upstream and downstream plenums of the micro-channel showed appreciable fluctuations that intensified with increasing heat flux. At high heat fluxes, these fluctuations were manifest by vapor surging upstream against the incoming liquid flow, resulting in dryout over much of the upstream region. The vapor was then pushed momentarily downstream by the liquid before surging upstream again. This process was repeated as wall temperature rose gradually at first and rapidly as CHF ensued. Fig. 6 depicts this vapor backflow pattern for the upstream region of the bare wall just before and at CHF.

IV. Experimental Results and Discussion

A. Boiling Curve Variations Along Heated Wall

Fig. 7 shows, for the bare copper wall, flow boiling curves obtained from temperature measurements at the four thermocouple locations (z_{tc1} to z_{tc4}) for a mass velocity of $G = 368$ kg/m^2.s and inlet temperature of $T_{\rm in} = 30°$C. The heat flux is plotted with respect to the difference between surface temperature at a particular thermocouple location, $T_{w,tci}$, and $T_{\rm in}$, where $T_{w,tci}$ is determined from the assumption of one-dimensional heat conduction between the corresponding thermocouple and the heated wall ($T_{w,tci} = T_{tci} - q'' H_{th}/k_s$).

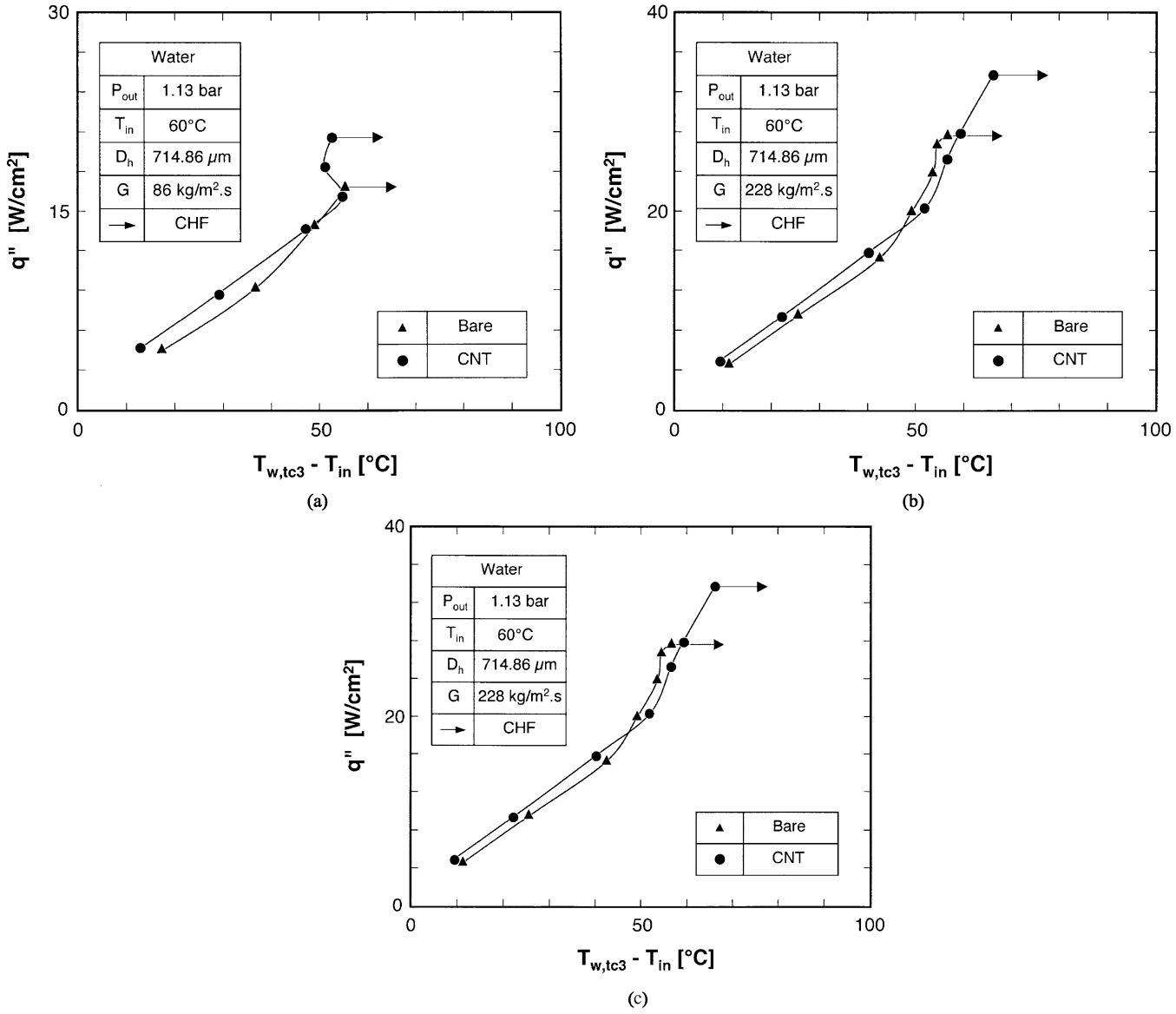

Fig. 9. Subcooled flow boiling curves measured at ztc3 for bare and CNT-coated walls at $T_{\rm in} = 60^{\circ}$C for (a) $G = 86$ kg/m^2.s, (b) $G = 288$ kg/m^2.s, and (c) $G = 368$ kg/m^2.s.

Fig. 7 shows that the boiling curves at all four surface locations maintain fairly constant slope in the single-phase region. An increase in slope marks the onset of boiling, which was first detected at the wall location above the thermocouple farthest from the inlet (z_{tc4}) and propagated forward with increasing heat flux. For certain heat fluxes above the incipient boiling heat flux, the thermocouple located farthest from the inlet, *tc4*, read lower temperatures than the upstream thermocouple *tc3*, apparently because of temperature fluctuations as more vapor was produced along the channel. At CHF, thermocouple *tc4* detected a rapid unsteady temperature rise. This effect propagated quickly upstream towards the inlet.

B. Comparison of Boiling Performances of Bare Copper Wall and CNT-Coated Wall

Fig. 8 compares flow-boiling curves for the bare copper wall and the CNT-coated wall for three values of mass velocity for $T_{\rm in} = 30^{\circ}$C. All boiling curves are based on surface temperature at one axial location, z_{tc3}. This location is chosen for its downstream location, and is preferred to z_{tc4}, where temperatures sometimes displayed appreciable fluctuation. Overall, the shape of the boiling curves for the CNT-coated wall is similar to that of the bare wall, except for a leftward temperature shift and different CHF values. Fig. 8(a) and (c) show higher single-phase heat transfer coefficients were achieved with the CNT-coated wall; this effect is negligible for the middle mass velocity of $G = 228$ kg/m^2.s. Anomalies in boiling curve trends might be related to morphological changes to the CNT-coating between tests. It should be noted that the low mass velocity test was performed first, followed, respectively, by the middle and high mass velocity tests. It is therefore possible that the boiling process altered the surface morphology in each test, and changes from a given test were still prevalent in subsequent test. This issue of the cumulative effect of flow boiling on surface morphology is discussed in a more recent article by the authors [17] involving

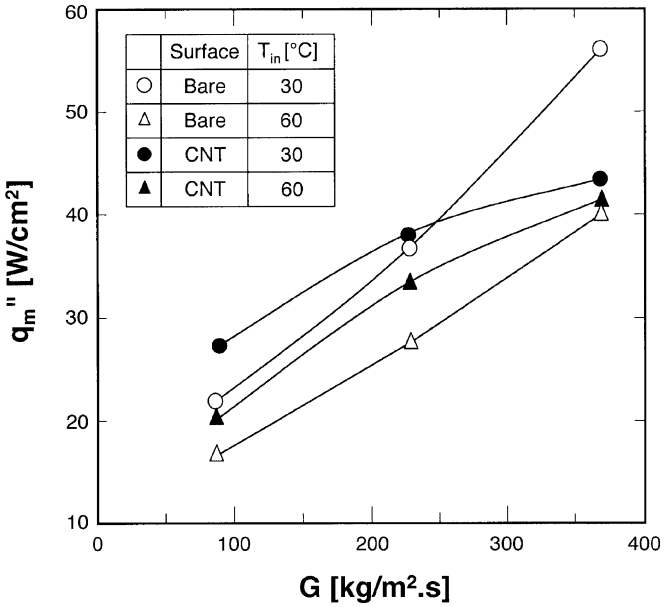

Fig. 10. Variation of CHF with mass velocity for bare and CNT-coated walls for inlet temperatures of 30°C and 60°C.

the use of a new surface for different tests. Fig. 8(a) and (c) demonstrate the single-phase enhancement is far more appreciable at the lower mass velocity of $G = 86$ kg/m^2.s than at 368 kg/m^2.s. In general, the CNT coating initiated boiling at a lower heat flux than the bare surface. In the nucleate boiling region, Fig. 8(a) shows appreciable heat transfer enhancement for the lowest mass velocity of $G = 86$ kg/m^2.s. However, the two higher mass velocities of $G = 228$ and 368 kg/m^2.s show poorer nucleate boiling performance for the CNT-coated surface. Fig. 8 shows a monotonic increase in CHF with increasing G for both surfaces.

Fig. 9 compares boiling curves for the bare and CNT-coated walls for the same three values of mass velocity at a higher inlet temperature of $T_{\rm in} = 60°$C, *i.e.*, lower subcooling. At this higher temperature, the CNT-coated wall enhanced the single-phase heat transfer coefficient for all three mass velocities. The enhancement was more appreciable for the lowest mass velocity of $G = 86$ kg/m^2.s and very small for $G = 368$ kg/m^2.s. Like Fig. 8, the CNT-coated wall provided significant two-phase enhancement for $G = 86$ kg/m^2.s but poorer performance at $G = 368$ kg/m^2.s.

Visual inspection following the boiling tests showed the CNT coating was well preserved compared to before the tests. However, there was a change of texture in certain regions. One difficulty in assessing the orientation, density, and quality of CNT anchoring to the wall was the large size of the copper block, which prevented the authors from obtaining SEM images of the surface. In a recent study by the authors [17], similar experiments were performed with several fresh CNT-coated surfaces for different mass velocities. The CNT-coated wall was sliced off from the copper block to obtain SEM images of the coating. These images showed no apparent loss of CNTs, proving the CNT anchoring was quite effective. However, these images revealed substantial morphological changes to the coating in the form of severe bending of CNTs, especially at high mass velocities.

TABLE III
PRESENT WATER CHF DATA FOR BARE SURFACE

T_{in} [°C]	G [kg/m^2.s]	q''_m [W/cm^2]
30.32	86	21.88
30.18	228	36.83
30.19	368	56.03
61.29	86	16.96
60.51	228	27.9
60.86	368	40.4

TABLE IV
PRESENT WATER CHF DATA FOR CNT-COATED SURFACE

T_{in} [°C]	G [kg/m^2.s]	q''_m [W/cm^2]
32.73	86	27
30.59	228	37.95
30.77	368	43.53
61.45	86	20.54
60.15	228	33.71
59.95	368	41.52

C. Comparison of CHF for Bare Copper Surface and CNT-Coated Surface

Fig. 10 shows the variation of CHF with mass velocity for both the bare and CNT-coated walls for the two inlet subcoolings. For the lowest mass velocity of 86 kg/m^2.s, the CNT-coated wall enhanced CHF by 23.4% at $T_{\rm in} = 30°$C and 21.1% at $T_{\rm in} = 60°$C. The enhancement diminished for the intermediate mass velocity of $G = 268$ kg/m^2.s to 3% for $T_{\rm in} = 30°$C and 20.8% for $T_{\rm in} = 60°$C. The CHF performance of the CNT-coated wall was further compromised at the highest mass velocity of $G = 368$ kg/m^2.s, yielding a 22.3% reduction in CHF for $T_{\rm in} = 30°$C and only 2.8% enhancement for $T_{\rm in} = 60°$C. Tables III and IV summarize the measured CHF values for the two walls.

D. Overall Assessment of CNT Enhancement Trends

Overall, it appears the enhancement benefits of CNTs are realized at low mass velocities but compromised at high mass velocities. At low mass velocities, it is hypothesized that CNTs maintain a near-vertical orientation and protrude further into the liquid flow, increasing both wall roughness and turbulence. However, high mass velocities are believed to cause significant folding of CNTs upon the heated wall, decreasing the wall roughness and turbulence compared to the low mass velocity.

In terms of boiling incipience, CNT arrays appear to be effective at both initiating and sustaining the nucleation process

by modifying the process of vapor embryo entrapment. As suggested by Ujereh *et al.* [10] for pool boiling, parallel vertical CNTs as well as the mesh of CNTs create deep, near-zero-angle cavities that are conducive of embryo formation. Ujereh *et al.* also suggested that CHF enhancement in pool boiling is the result of increased surface area. For the present study, the trends of incipient boiling and CHF for the CNT-coated surface are consistent with those for pool boiling only at low mass velocity.

Poorer enhancement at high mass velocities is probably related to the effects of coolant flow on CNT arrays. CNTs possess very high axial strength, but high flow velocities fold CNTs towards the wall, excepting surfaces that are coated with very dense CNT arrays. Such an effect reduces the depth of CNT-mesh-induced cavities, compromising the effectiveness of CNTs at capturing and sustaining embryos both at the onset of boiling and throughout the nucleate boiling region.

At CHF, CNT arrays provide two key enhancement mechanisms. First, as suggested by Ujereh *et al.*, they increase heat transfer area. Second, CNT arrays serve as very high conductivity fins that penetrate into the cooler, bulk liquid and take advantage of the bulk subcooling away from the wall. These two mechanisms are prevalent at low mass velocities, but weakened at high mass velocities. This explains the CHF trends depicted in Fig. 10 for the CNT-coated wall compared to the bare wall.

The present study showed slightly higher single-phase pressure drop at low mass velocity for the CNT-coated wall compared with the bare wall. However, the pressure drop differences increased with increasing mass velocity. This trend might be explained by the flow obstruction and increased turbulence caused by the CNT structures.

V. Conclusion

This study explored the thermal benefits of coating the bottom wall of a shallow rectangular micro-channel with CNTs. Experiments were performed with both a bare copper wall and a CNT-coated copper wall at different mass velocities and two inlet temperatures using deionized water as working fluid. Boiling curves were generated for both surfaces to explore key performance parameters such as the onset of boiling, the nucleate boiling heat transfer coefficient and wall superheat, and CHF. High-speed video imaging was used to capture interfacial behavior and dominant two-phase flow pattern development along the micro-channel for the different operating conditions. Key findings from this study are as follows.

1) For both the bare and CNT-coated walls, boiling commenced in the downstream region of the micro-channel in the form of bubbles that nucleated mostly towards the sidewalls. The CNT-coated wall initiated boiling at a lower heat flux and with greater abundance and intensity. At high heat fluxes, strong fluctuations in both the inlet and outlet pressure were observed for both surfaces. Ultimately, the vapor surged upstream against the incoming liquid flow, resulting in dryout over much of the upstream region. This vapor backflow was a precursor to CHF for both wall types.
2) CNT arrays enhanced the single-phase heat transfer coefficient, especially for low mass velocities. Similar enhancement was achieved in the nucleate boiling region for low mass velocities. However, high mass velocities compromised or eliminated altogether any enhancement in the nucleate boiling region. The enhancement achieved at low mass velocities appears to be the result of deep, near-zero-angle cavities formed by vertical CNTs as well as the mesh of CNTs. On the other hand, high flow velocities tend to fold CNTs upon the heated wall, reducing the depth of CNT-mesh-induced cavities and compromising the effectiveness of CNTs at capturing and sustaining embryos both at the onset of boiling and throughout the nucleate boiling region.
3) CHF enhancement was also achieved with CNT arrays mostly at low mass velocities. For the lowest mass velocity of 86 kg/m^2.s, the CNT arrays enhanced CHF by 23.4% at $T_{\rm in} = 30^{\circ}$C and 21.1% at $T_{\rm in} = 60^{\circ}$C. On the other hand, CHF performance for $G = 368$ kg/m^2.s was 22.3% lower than for the bare wall at $T_{\rm in} = 30^{\circ}$C and only 2.8% better than the bare wall at $T_{\rm in} = 60^{\circ}$C. It is postulated CNT arrays enhance CHF by increasing heat transfer area as well as by serving as very high conductivity fins that penetrate into the cooler, bulk liquid and take advantage of the bulk subcooling away from the wall. While these two mechanisms are prevalent at low velocities, they are both weakened at high mass velocities, especially the fin effect, because of the folding of CNT arrays upon the wall.
4) While the present study provides valuable insight into the enhancement benefits of CNT coatings to flow boiling, additional research is required to better understand such important issues as the influence of the CNT coating on pressure drop, surface changes following repeated tests, and the influence of these changes on the repeatability of boiling performance. These issues are presently under study by the authors.

References

[1] I. Mudawar, "Assessment of high-heat-flux thermal management schemes," *IEEE Trans. Compon. Packag. Technol.*, vol. 24, pp. 122–141, 2001.
[2] I. Mudawar and D. E. Maddox, "Critical heat flux in subcooled flow boiling of fluorocarbon liquid on a simulated electronic chip in a vertical rectangular channel," *Int. J. Heat Mass Transfer*, vol. 32, pp. 379–394, 1989.
[3] T. C. Willingham and I. Mudawar, "Forced convection boiling and critical heat flux from a linear array of discrete heat sources," *Int. J. Heat Mass Transfer*, vol. 35, pp. 2879–2890, 1992.
[4] W. Qu and I. Mudawar, "Measurement and correlation of critical heat flux in two-phase micro-channel heat sinks," *Int. J. Heat Mass Transfer*, vol. 47, pp. 2045–2059, 2004.
[5] W. Qu and I. Mudawar, "Transport phenomena in two-phase micro-channel heat sinks," *ASME J. Electron. Packag.*, vol. 126, pp. 213–224, 2004.
[6] W. Qu and I. Mudawar, "Flow boiling heat transfer in two-phase micro-channel heat sinks-I. experimental investigation and assessment of correlation methods," *Int. J. Heat Mass Transfer*, vol. 46, pp. 2755–2771, 2003.
[7] M. E. Steinke and S. G. Kandlikar, "An experimental investigation of flow boiling characteristics of water in parallel microchannels," *ASME J. Heat Transfer*, vol. 126, pp. 518–526, 2004.
[8] G. Wang, P. Cheng, and H. Wu, "Unstable and stable flow boiling in parallel microchannels and in a single microchannel," *Int. J. Heat Mass Transfer*, vol. 50, pp. 4297–4310, 2007.
[9] P. Kim, L. Shi, A. Majumdar, and P. L. McEuen, "Thermal transport measurements of individual multiwalled nanotubes," *Phys. Rev. Lett.*, vol. 87, pp. 1–4, 2001.

[10] S. Ujereh, T. Fisher, and I. Mudawar, "Effects of carbon nanotube arrays on nucleate pool boiling," *Int. J. Heat Mass Transfer*, vol. 50, pp. 4023–4038, 2007.
[11] S. Launay, A. G. Fedorov, Y. Joshi, A. Cao, and P. M. Ajayan, "Hybrid micro-nano structured thermal interfaces for pool boiling heat transfer enhancement," *Microelectron. J.*, vol. 37, pp. 1158–1164, 2006.
[12] E. Dujardin, T. W. Ebbesen, H. Hiura, and K. Tanigaki, "Capillarity and wetting of carbon nanotubes," *Science*, vol. 265, pp. 1850–1852, 1994.
[13] J. Xu and T. S. Fisher, "Enhancement of thermal interface materials with carbon nanotube arrays," *Int. J. Heat Mass Transfer*, vol. 49, pp. 1658–1666, 2006.
[14] B. A. Cola, J. Xu, C. Cheng, H. Hu, X. Xu, and T. S. Fisher, "Photoacoustic characterization of carbon nanotube array thermal interfaces," *J. Appl. Phys.*, vol. 101, 2007.
[15] M. Meyyappan, L. Delzeit, A. Cassell, and D. Hash, "Carbon nanotube growth by PECVD: A review," *Plasma Sources Sci. Technol.*, vol. 12, pp. 205–216, 2003.
[16] M. R. Maschmann, P. B. Amama, A. Goyal, Z. Iqbal, R. Gat, and T. S. Fisher, "Parametric study of synthesis conditions in plasma-enhanced CVD of high-quality single-walled carbon nanotubes," *Carbon*, vol. 44, pp. 10–18, 2006.
[17] V. Khanikar, I. Mudawar, and T. S. Fisher, "Effects of carbon nanotube coating on flow boiling in a micro-channel," *Int. J. Heat Mass Transfer*, to be published.

Vikash Khanikar received the B.S. and M.S. degrees in mechanical engineering from Purdue University, West Lafayette, IN, in 2006 and 2008, respectively. His graduate work focused on flow boiling effects of coating the bottom wall of a micro-channel with CNTs.

He is currently working as a Thermal Engineer for Hewlett-Packard Company, Houston, TX.

Issam Mudawar received the M.S. and Ph.D. degrees from the Massachusetts Institute of Technology, Cambridge, in 1980 and 1984, respectively. His graduate work involved magnetohydrodynamic (MHD) energy conversion and phase-change water cooling of turbine blades.

He joined the Purdue University School of Mechanical Engineering, West Lafayette, IN, in 1984, where he established, and became Director of, the Boiling and Two-Phase Flow Laboratory (BTPFL) and Purdue University International Electronic Alliance (PUIECA). His work has been focused on phase change processes, thermal management of electronic and aerospace devices, intelligent materials processing, hydrogen storage, high-Mach turbine engines, and nuclear reactor safety. His theoretical and experimental research encompasses sensible and evaporative heating of thin films, pool boiling, flow boiling, jet-impingement cooling, spray cooling, micro-channel heat sinks, heat transfer enhancement, heat transfer in rotating systems, critical heat flux, and capillary pumped flows. He is also President of Mudawar Thermal Systems, Inc., a firm that is dedicated to the development of thermal management solutions.

Prof. Mudawar received several awards for his research accomplishments, including Best Paper Award in Electronic Cooling at the 1988 National Heat Transfer Conference, Best Paper Award in Thermal Management at the 1992 ASME/JSME Joint Conference on Electronic Packaging, the *Journal of Electronic Packaging* Outstanding Paper of the Year Award for 1995, and the Best Paper Award in Thermal Management at ITherm 2008. He also received several awards for excellence in teaching and service to Purdue students and their organizations, including the Solberg Award for Best Teacher in School of Mechanical Engineering (1987, 1992, 1996, and 2004), the Charles Murphy Award for Best Teacher at Purdue University (1997), and the National Society of Black Engineers Professor of the Year Award (1985 and 1987). He was named Fellow of the American Society of Mechanical Engineers (ASME) in 1998.

Timothy S. Fisher received the B.S. and Ph.D. degrees in mechanical engineering from Cornell University, Ithaca, NY, in 1991 and 1998, respectively.

He joined the Purdue's School of Mechanical Engineering and Birck Nanotechnology Center, West Lafayette, IN, in 2002 after several years at Vanderbilt University. Prior to his graduate studies, he was employed from 1991 to 1993 as a design engineer in Motorola's Automotive and Industrial Electronics Group. His research has included efforts in simulation and measurement of nanoscale heat transfer, coupled electrothermal effects in semiconductor devices, nanoscale direct energy conversion, molecular electronics, microfluidic devices, hydrogen storage, and computational methods ranging from atomistic to continuum scales. Applications of his work cover a broad range of areas, including nanoelectronics, thermal interface materials, thermal–electrical energy conversion, biosensors, and hydrogen storage.

Dr. Fisher serves on the IEEE TC-9 Committee on Thermal Phenomena in Electronics, the ASME K-6 committee on Heat Transfer in Energy Systems, ASME K-16 Committee on Thermal Management of Electronics, and is a member of the Tau Beta Pi and Pi Tau Sigma honor societies.